Food Chemistry 514 (2026) 149100

Contents lists available at ScienceDirect

Food Chemistry

journal homepage: www.elsevier.com/locate/foodchem

Ulvan acts as a prebiotic polysaccharide enhancing the production of indoles and short-chain fatty acids *in vitro*: a metabolomics study

Beatrice Zonfrillo [a,c,*], Carmen M.S.Ambrosio [b], Nadia Mulinacci [a], Josep Rubert [b,c,*]

[a] Department of Neurosciences, Psychology, Drug Research and Child Health (NEUROFARBA), University of Florence, Via Ugo Schiff 6, Sesto Fiorentino, Italy
[b] Division of Human Nutrition and Health, Wageningen University & Research, Stippeneng 4, Wageningen, the Netherlands
[c] Food Quality and Design group, Wageningen University & Research, P. O. Box 17, 6700, AA, Wageningen, the Netherlands

A B S T R A C T

This study investigated the fermentability and prebiotic potential of ulvan, a sulfated polysaccharide from *Ulva lactuca* L., using an *in vitro* human colonic fermentation model. Targeted metabolomics quantified SCFA and tryptophan-derived metabolites to assess saccharolytic activity and fiber-driven modulation of amino acid metabolism.

Ulvan supplementation significantly stimulated SCFA production, particularly acetic acid, achieving levels comparable to the well-established prebiotic inulin. In parallel, ulvan selectively modulated tryptophan metabolism, enhancing the production of health-associated metabolites such as indole-3-propionic acid and indole-3-acetic acid, suggesting cross-feeding interactions among saccharolytic and indole-producing taxa. Untargeted metabolomics revealed distinct metabolites associated with ulvan treatment, including cyclic proline dipeptides, which points to a selective stimulation of beneficial microbial species.

Collectively, these findings demonstrate that ulvan is a soluble and fermentable dietary fiber, supporting its potential as a functional food ingredient or dietary supplement for promoting gut health.

1. Introduction

Ulvan is a unique, sulfated polysaccharide present in the cell walls of green macroalgae of Ulvaceae family. It consists mainly of repeating units of rhamnose-3-sulfate (Rha3S), linked to D-glucuronic acid (GlcA), L-iduronic acid (IdoA), or D-xylose (Xyl) (Kidgell et al., 2019). Among *Ulva* species; *U. lactuca* L. (sea lettuce) is one of the most widespread macroalgae worldwide and is receiving increasing attention due to its involvement in green tides – extensive blooms associated with coastal eutrophication; which raise issues of biomass management (Beer, 2023). In addition to its ecological role; *Ulva* has been approved in Europe as both a food and a food supplement and represents a valuable source of bioactive compounds; making its biomass an attractive target for valorization and practical applications (Araújo & Peteiro, 2021). Isolated ulvan has also been investigated for food technological applications; for example; as an emulsifier and stabilizer agent in oil-in-water emulsions in soft drinks (Morelli et al., 2019); and symbiotic yogurt production; improving viscosity; firmness; and the growth of probiotic bacteria (Shalaby & Amin, 2019). Recent *in vivo* studies further reported ulvan's antihyperglycemic effects in a murine model of aging-related diabetes (Ruan et al., 2023); and its anti-inflammatory and immunoregulatory properties in a murine model of DNBS-induced colitis (Ardizzone et al., 2023).

Ulvan has been reported as a soluble dietary fiber (Lahaye & Jegou, 1993); which could be utilized and fermented by the human gut microbiota. Fermentability of a polysaccharide refers to the ability of gut microorganisms to metabolize the polysaccharide; depolymerizing it and producing end-products; such as short-chain fatty acids (SCFA) through saccharolytic activity (Holscher, 2017). To date; studies on ulvan fermentability have shown contrasting results. Early studies found that SCFA production during *Ulva* or ulvan fermentation was low; comparable to the employed growth controls (Durand et al., 1997; Kong et al., 2016). By contrast, more recent *in vitro* studies involving fecal fermentations have reported the production of acetate and lactate, along with the enrichment of the beneficial bacterial taxa *Bifidobacterium* and *Lactobacillus*, suggesting the prebiotic potential of ulvan (Seong et al., 2019). The variability observed among these studies may correspond to the different metabolic responses to dietary fibers; which are indeed not uniform across individuals but are strongly influenced by the initial structure and functionality of microbial communities (Dell'Olio et al., 2024; Murga-Garrido et al., 2021). The structural complexity of ulvan also plays a role in its fermentability, as ulvan requires specific carbohydrate-active enzymes (CAZymes) for degradation, which are primarily encoded by *Bacteroides spp.*, the primary degraders of complex

* Corresponding authors at: Food Quality and Design group, Wageningen University & Research, P. O. Box 17, 6700, AA, Wageningen, the Netherlands.
E-mail addresses: beatrice.zonfrillo@unifi.it (B. Zonfrillo), josep.rubert@wur.nl (J. Rubert).

https://doi.org/10.1016/j.foodchem.2026.149100
Received 16 October 2025; Received in revised form 16 March 2026; Accepted 30 March 2026
Available online 31 March 2026

polysaccharides (Gotteland et al., 2020).

The prebiotic capacity of ulvan, defined as the selective utilization of a substrate by host microorganisms that confers a health benefit (Gibson et al., 2017); remains debated. Most studies have focused solely on SCFA production or microbial composition; yet the health benefits of prebiotic fibers may also result from other microbial pathways. In particular; fermentable dietary fibers are increasingly recognized to influence microbial metabolism beyond carbohydrate utilization; affecting interconnected metabolic pathways. Primary degraders of complex polysaccharides can initiate cross-feeding interactions; providing oligosaccharides; monosaccharides; and SCFA to other beneficial gut commensals such as *Bifidobacterium* (Cherry et al., 2019). Significantly; these interactions may extend beyond saccharolytic fermentation and influence the availability and utilization of amino acids; including the microbial catabolism of tryptophan (Huang et al., 2024; Sinha et al., 2024). Tryptophan-derived metabolites are increasingly recognized as key mediators of host–microbiota interactions, intestinal homeostasis, and immune modulation (Agus et al., 2018; Roager & Licht, 2018). To date, however, no studies have addressed whether ulvan can influence tryptophan metabolism or drive the production of bioactive indole-derived metabolites beyond SCFA.

Based on this background, we hypothesize that ulvan can be fermented by the human gut microbiota and also influence other microbial metabolic pathways, including tryptophan microbial catabolism, through saccharolytic activity and cross-feeding interactions. The aim of this study was therefore to investigate the fermentation of ulvan extracted from *U. lactuca* L. using an *in vitro* human colonic model with fecal inocula from four donors. Ulvan fermentation was compared with inulin, a well-established prebiotic, to clarify whether ulvan exhibits similar or distinct metabolic dynamics. To obtain a comprehensive understanding of the metabolic outcomes, we employed a combination of targeted and untargeted metabolomics. Specifically, we quantified SCFA as markers of carbohydrate fermentation and evaluated tryptophan-derived metabolites as indicators of fiber-driven modulation of amino acid metabolism. In addition, branched-chain fatty acids (BCFA), derived from microbial protein fermentation (Gozdzik et al., 2023), were also quantified to provide a more complete picture of the balance between saccharolytic and proteolytic processes during the *in vitro* fermentation. Finally, untargeted metabolomics was employed to characterize broader shifts in the colonic metabolome and to gain additional insights into the metabolic impact of ulvan.

2. Material and methods

2.1. Materials and reagents

The following reagents were purchased from Merck KGaA (Darmstadt, Germany): 2-ethylbutyric acid (#109959), butyric acid (#19215), isovaleric acid (#78651), propionic acid (#8.00605), isobutyric acid (#I1754), valeric acid (#240370), formic acid (#33015-M), oxalic acid (#75688), bile extract porcine (#B8631), L-cysteine HCl (#2430-M), mucine from porcine stomach (#M2378), porcine pepsin (#P6887), porcine pancreatin 4USP (#P1750), K_2HPO_4 (#1.09828), KH_2PO_4 (#1.04871), $NaHCO_3$ (#S5761), Tween-80 (#P8074), sodium thioglycolate (#T0632), $Na_2S_2O_4$ (#1.06507), $CaCl_2 \bullet 2H_2O$ (#223506), NaOH (#1.06498), KCl (#P5405), NaCl (#S5886), $MgCl_2 \bullet 6H_2O$ (#M2393), $(NH_4)_2CO_3$ (#1.59504). MS grade MeOH (#85800), and HCl (#20252.290) were purchased from VWR International Srl (Radnor, PA, USA). The following reagents were purchased from Thermo Fisher Scientific Inc. (Waltham, MA, USA): yeast extract (#LP0021), peptone special (#LP0072B), inulin from chicory root (#457101000), Slide-A-Lyzer™ Dialysis Cassettes (10 K MWCO, #66830). Milli-Q water was produced by Milli-Q PURELAB Ultra, ELGA LabWater (Lane End, U.K.).

2.2. Ulvan

U. lactuca L. sample was collected in August 2022 in the aquaculture tank of Pescatori Orbetello cooperative, in the Orbetello lagoon, Tuscany, Italy. The algae were sun-dried for one day and stored under vacuum. Ulvan was extracted with HCl 0.01 M 60 mL/g at 100 °C for 105 min under magnetic stirring according to a recently optimized protocol (Zonfrillo, Bellumori, Digiglio, et al., 2025). Polysaccharides were precipitated with 3 volumes of EtOH, dialyzed with a 10 kDa cassette, and freeze-dried.

Constituent monosaccharide composition was evaluated by HPAEC-PAD after double hydrolysis (2 M anhydrous HCl in MeOH, 100 °C, 5 h, followed by 2 M TFA, 120 °C, 1 h) (De Ruiter et al., 1992; Zonfrillo, Bellumori, Digiglio, et al., 2025). Sulfate content was measured by turbidimetric assay with the barium chloride-gelatin method (Torres et al., 2021). NMR spectra were acquired with a Bruker 400 MHz spectrometer. Bruker pulse sequences "zg" (D1: 35 s, pulse width: 7.50 μs, ns: 32) and "noesygppr1d" (D1: 35 s; pulse width: 7.66 μs; ns: 32) were used. All measurements were performed at 298 K. MestReNova 14.2.1 software was used for data processing.

2.3. In vitro digestion

The *in vitro* simulated gastrointestinal digestion was performed with the standard INFOGEST protocol reported by Brodkorb et al. (2019). The experimental design included ulvan; inulin; which was chosen as a positive control due to its well-established prebiotic effects as a fermentable fiber (Gill et al., 2021), and a blank sample. Briefly, 1 g of ulvan or inulin was suspended in 5 mL of ultrapure water and subjected to a simulated salivary phase (pH 7.0 ± 0.1) for 2 min, simulated gastric phase (pH 3.0 ± 0.1) for 2 h and simulated intestinal phase (pH 7.0 ± 0.1) for other 2 h. Blank digestion was performed starting with 5 mL of ultrapure water. Samples were incubated at 37 °C in a rotator (Multi RS-60, Biosan SIA, Riga, Latvia). After the intestinal phase, samples were heat-shocked at 100 °C for 5 min for enzyme inactivation and then freeze-dried. The composition of the simulated salivary, gastric and intestinal phases is shown in Table S1.

2.4. In vitro batch colonic fermentation

Fermentation of digested ulvan, inulin and blank (growth control) samples was performed according to Pérez-Burillo et al. (2021) with some modifications.

Fresh fecal samples were collected from 4 donors, three female and one male, 25–30 years old, with a body mass index between 18.5 and 25, located in Wageningen (The Netherlands) and its surroundings. All donors were in good health, omnivorous, not smokers, and with no history of gastrointestinal disorders or antibiotics treatment for at least 6 months before this study. The healthy volunteers gave consent for a single fecal donation, and their anonymity was granted. According to the guidelines of the Medical Ethical Advisory Committee of Wageningen University (METC-WU), this research did not require ethical approval (Registration Number METC 2024–17,059). Moreover, this research was conducted in agreement with the WMA Declaration of Helsinki about Ethical Principles for Medical Research Involving Human Subjects.

All reagents, equipment, and digested samples were autoclaved or sterile-filtered before use and the whole procedure was done in aseptic conditions. Fresh fecal samples were collected in a collection box with an anaerobic bag and cryo-preserved right after the collection. For cryopreservation, fecal samples were mixed with glycerol:H_2O 1:1 (20% *w/v*) inside of a laminar flow cabinet and stored immediately at −80 °C. Feces were not pooled to assess biological variability. The day of the fermentation, slurries were thawed and centrifuged at 4000 *g*, 4 °C for 10 min to remove the cryopreservation solution. After centrifugation, the supernatants were discarded. The slurries were resuspended in

sterile phosphate buffer 20% *w/v* (pH 7.0 ± 0.05, 8.8 g/L K_2HPO_4, 6.8 g/L KH_2PO_4, 0.1 g/L sodium thioglycolate and 15 mg/L $Na_2S_2O_4$ sterile-filtered and added right before use), homogenized for 10 min at 300 *g* with a Bag Mixer (Stomacher® 400 circulator, Seward Ltd., Worthing, UK) and then centrifuged at 550 *g* for 5 min. Next, the supernatant was used as inoculum.

The batch fermentation was performed in 10 mL penicillin bottles containing 4.3 mL basal nutrient medium (5.22 g/L K_2HPO_4, 16.32 g/L KH_2PO_4, 2 g/L $NaHCO_3$, 2 g/L yeast extract, 2 g/L peptone, 1 g/L mucin, 2 mL/L Tween-80 and 0.5 g/L L-cysteine HCl sterile-filtered and added right before use) and 2 mL of corresponding treatment solution 3.5% *w/v* of digested blank, inulin, or ulvan (autoclaved beforehand). The treatment concentration in the final volume was 1% w/v. Bottles were sealed with butyl-rubber stoppers and aluminum caps, then flushed with N_2 for 30 min to create anaerobic conditions. Next, 0.7 mL of the fecal inoculum was added to the bottles using a sterile syringe. The digested blank plus the fecal inoculum was the growth control. Additionally, a blank of the fermentation was set and comprised the digested blank solution and phosphate buffer instead of fecal inoculum. After inoculation, the bottles were incubated at 37 °C with mild shaking and sampling was carried out at 0, 12, 24, and 48 h of fermentation. At those time points, fermentation was stopped by liquid N_2 shock, then the samples were thawed, aliquoted for the different analyses, and stored at −80 °C.

2.5. pH measurement

The pH of all samples was determined using a pH meter (VWR® pHenomenal pH1000L). Before performing the measurement, the pH meter was calibrated with three standard solutions at pH 4.01, 7.01, and 10.01 (Sigma-Aldrich).

2.6. Gel permeation chromatography

The molecular weight of ulvan and fermented ulvan samples at 0, 24, and 48 h was determined by High-Performance Gel Permeation Chromatography (HPGPC). Samples (5 mg) were dissolved in 1 mL of ultrapure water and filtered through a 0.22 μm filter membrane.

The HPGPC system consisted of an Ultimate 3000 HPLC (Thermo Fisher Scientific, MA, US) with three TSK-GEL columns connected in series (4000–3000-2500 SuperAW; 150 × 6 mm) and a TSK-Gel guard column (TSKgel Guardcolumn SuperSW, 6 mm ID × 40 mm). The system was coupled with an RI detector (RefractoMax520, Thermo Fisher). Column oven was set at 55 °C. A mobile phase consisting of 0.2 M $NaNO_3$ solution was used at a flow rate of 0.6 mL min^{-1}. A standard curve was obtained by various pullulan standards (MWs of 6.1, 21.1, 47, 107, 194, 344 kDa) plotting retention time *vs* log(MW). Data analysis was performed on Chromeleon 7.3.1.3 (Thermo Fisher Scientific Inc., San Jose, CA).

2.7. Short-chain fatty acids analysis

For SCFA analysis the samples were centrifuged at 4 °C, 9000 *g* for 5 min, and the supernatants were filtered with 0.2 μm RC filter and stored at −80 °C. Before injection, the frozen supernatants were defrosted at 4 °C and then mixed with the internal standard solution (0.9 mg/mL 2-ethylbutyric acid in 0.3 M HCl and 0.9 M oxalic acid) at a ratio of 8:1 (*v/v*). Quantification was performed on a Shimadzu GC-2014 (Kyoto, Japan) equipped with a flame ionization detector as previously described (Huang, Boekhorst, et al., 2023).

2.8. Tryptophan-related metabolites analysis

Tryptophan and indole derivatives were measured *via* a Nexera XR LC-20ADxr UPLC system equipped with an autosampler X2 SIL-30 AC, a column oven CTO-20 AC, and coupled with an LCMS-8050 mass spectrometer (Shimadzu Corporation, Kyoto, Japan). A Kinetex® 1.7 μm EVO C18 column (100 Å, 100 × 2.1 mm) (Phenomenex, Torrance, USA), was used for the chromatographic separation and heated at 45 °C. The mobile phase consisted of solvent A (100% H_2O + 0.1% FA) and solvent B (100% MeOH +0.1% FA), with a flow rate of 0.3 mL min^{-1}. The elution program was set as follows: 0–2 min, 0.1% B; 2–5 min 0.1–90% B; 5–8 min 90% B; 8–9 min 90–0.1% B; 9–14 min 0.1% B.

The metabolites, including Trp (Rt 6.02 min), kynurenine (Kyn; Rt 3.15 min), serotonin (5-HT; Rt 4.56 min), tryptamine (TA; Rt 6.65 min), oxindole (Oxi; Rt 6.78 min), indole-3- lactic acid (ILA; Rt 6.92 min), indole-3-aldehyde (I3A; Rt 7.05 min), indole-3-acetic acid (IAA; Rt 7.15 min), indole-3-propionic acid (IPA; Rt 7.43 min), indole (Ind; Rt 7.50 min), 3-indoleacrylic acid (IA; Rt 7.52), and 3-methylindole (3 M; Rt 7.43 min), were quantified in the multiple reaction monitoring mode according to a method described elsewhere (Huang, Boekhorst, et al., 2023).

For the analysis, samples were centrifuged at 4 °C, 9000 *g* for 5 min, and the supernatants were filtered with 0.2 μm RC filter before injection (10 μL). For the tryptophan quantification, samples were diluted from 25 to 50 times according to the Trp concentration. Data analysis was performed on LabSolutions Insight (Shimadzu Corporation, Japan).

2.9. Untargeted metabolomics

For untargeted analysis, extraction of polar and medium polar metabolites was carried out on ulvan, growth control and inulin samples. Metabolites from 1 mL of the samples were extracted with 0.3 mL MeOH followed by two cycles of vortex (1 min) - snap freezing with liquid N_2, and sonication for 10 min at low temperature. After the extraction, samples were stored at −20 °C for 1 h to promote protein precipitation, then centrifuged at 12557 *g* for 10 min at 5 °C to collect the supernatants. Blank extractions were performed using 1 mL of ultrapure water. Quality control (QC) samples were prepared by mixing 20 μL of all extracts (excluding the extraction blanks).

LC-MS/MS analysis was carried out with a Nexera XS UHPLC system with a DGU-405 degassing unit, an LC-40D XS solvent delivery pump, a SIL-40C XS autosampler, a CTO-40S column oven, and a CBM-40 lite system controller (Shimadzu Corporation, Kyoto, Japan). The UHPLC was coupled with a QTOF mass spectrometer with an electrospray ionization source (LCMS-9030, Shimadzu Corporation, Kyoto, Japan). An Acquity UPLC BEH C18 column® (1.7 μm, 2.1 × 100 mm) with an Acquity UPLC BEH C18 VanGuard Pre-column (1.7 μm, 2.1 × 5 mm) (Waters Corporation, Milford, Massachusetts, USA) was used for the chromatographic separation and heated at 40 °C. The mobile phase consisted of solvent A (100% H_2O + 0.1% FA) and solvent B (100% MeOH +0.1% FA), with a flow rate of 0.3 mL min^{-1}. The elution program and MS parameters were set according to Izquierdo-Sandoval et al. (2024). To minimize any potential bias from instrumental drift, the samples were injected in random order. The sequence was arranged to start with 10 extraction blanks, followed by 5 injections of QCs. Thereafter, one QC and one extraction blank were injected into every ten samples. Two external standards (hesperidin and sulphaguanidine) were injected every 25 runs to ensure the reproducibility of retention times and accurate mass measurements.

2.10. Data processing and statistical analysis

2.10.1. Targeted data

Differences between treatments at the same time point, as well as among time points within each treatment, were assessed using a two-way ANOVA, following a randomized block design. The analysis was conducted in RStudio version 4.2.2, utilizing the AgroR package (Shimizu et al., 2024).

For non-parametric responses, rank-transformed data were analyzed *via* ANOVA using the ARTool package (Elkin et al., 2021; Kay et al., 2021; Wobbrock et al., 2011) in RStudio. Post-hoc comparisons were performed with Tukey's test, with significance set at $p < 0.05$.

Repeated-measures ANOVA simultaneous component analysis (RM-ASCA) was conducted with the ALASCA package in RStudio (Jarmund et al., 2022).

The regression model was specified in Eq 1

$$Time + Treatment + Time : Treatment + (1|ID) \quad (1)$$

where the terms *Time* and *Treatment* represent the main effects of time and treatment, respectively, while *Time:Treatment* represents their interaction. The random intercept *(1|ID)* accounts for inter-individual variability, allowing each donor to have their own baseline level of the dependent variable. Data preprocessing included scaling by dividing the values of each variable by the standard deviation across all samples, followed by log transformation. Model validation was conducted using a bootstrapping method with a jackknife procedure ($n = 1000$). Confidence intervals (CIs) for scores and loadings were determined by selecting the 2.5% and 97.5% percentiles from the bootstrap validation runs.

2.10.2. Untargeted data

UHPLC-QTOF MS raw data (.lcd files) were first converted into centroid .mzML format using the msConvert tool in ProteoWizard (Chambers et al., 2012) and imported into MZMINE 3 (version 4.0.8) for data processing. The workflow included smoothing; peak peaking; alignment; and gap filling (Schmid et al., 2023). Feature detection was performed within a retention time (Rt) window of 1–16 min; with *m/z* tolerances set to 20 ppm for scan-to-scan; 3 ppm for intra-sample; and 8 ppm for sample-to-sample. Rt tolerances were set to 0.04 min for intra-sample and 0.10 min for sample-to-sample alignments. Noise thresholds were set at 1000 and 100 for MS1 and MS2; respectively. Data quality was subsequently assessed by inspecting Principal Component Analysis (PCA) scores plots in MetaboAnalyst 6.0 (González-Domínguez et al., 2024; Pang et al., 2024).

The aligned dataset was further processed with Sirius 5.8.6 for feature annotation. Several sub tools within Sirius were employed, including molecular formula annotation (SIRIUS + ZODIAC), molecular fingerprint prediction and compound class prediction (CSI:FingerID + CANOPUS), and structure database search (CSI:FingerID + COSMIC) (Dührkop et al., 2015; Dührkop et al., 2019; Dührkop et al., 2021; Hoffmann et al., 2022; Ludwig et al., 2020). For the CSI:FingerID Structure Database Search, all available databases were selected except PubChem.

To ensure a high-confidence dataset, the generated matrices were filtered carefully. Only formula-annotated features meeting the following criteria were retained: *(i)* precursor mass error $< |5|$ ppm; *(ii)* median fragment mass error $< |10|$ ppm; and *(iii)* relative explained intensity of MS/MS spectra >0.7. These features, annotated with the molecular formula, MS/MS spectrum, and CANOPUS classification, were assigned a Metabolomics Standards Initiative (MSI) confidence level of 3 according to Schymanski et al. (2014). For features with database matches, additional filters were applied, retaining only those with a formula rank <4 and a COSMIC Confidence Score > 0.4. CANOPUS classification was subsequently integrated for these features with a MSI confidence level of 2a.

A combined matrix containing features of confidence levels 2–4, along with their corresponding peak intensities, was then created. This matrix was further refined by retaining only features with high repeatability in QC injections (RSD < 20%) and significant variance across experimental conditions, determined using interquartile range (IQR) filtering to exclude the bottom 40% of features with minimal variability.

The final dataset, comprising samples of ulvan, inulin, and growth controls, was analyzed using the ALASCA package under the same settings previously reported for targeted data. Significant features identified by the RM-ASCA model and tentatively annotated by Sirius were further explored using microbeMASST (https://masst.gnps2.org/microbemasst/) to investigate potential microbial producers of these metabolites (Zuffa et al., 2024). Fig. S1 reports a schematic representation of the workflow carried out.

3. Results and discussion

After characterizing the structure and composition of the isolated ulvan, we initially evaluated its stability during *in vitro* digestion. We then conducted an *in vitro* colonic fermentation to evaluate both the fermentability of ulvan and its capacity to modulate gut microbial metabolism. To capture these effects, targeted and untargeted metabolomics were employed, allowing for both the quantification of specific metabolites and a broader characterization of the metabolic shift induced by ulvan. Thus, this integrative approach provides novel functional insights of ulvan fermentation moving beyond the evaluation of only conventional fermentation endpoints such as SCFA production (Charoensiddhi et al., 2022; Seong et al., 2019) or 16S rRNA–based taxonomic shifts (Kansandee et al., 2024; Kong et al., 2016; Seong et al., 2019).

3.1. Ulvan characterization

The ulvan sample, extracted from *U. lactuca* and purified by dialysis, yielded 11.43%. Its purity, expressed as the sum of total monosaccharides and sulfate groups, was estimated to be 78%, based on monosaccharide composition analysis and sulfate quantification. Its chemical composition (Table 1) and 2D-NMR analysis (as reported in Zonfrillo, Bellumori, Digiglio, et al., 2025) confirmed the typical structure of ulvan; consistent with previous literature (Chi et al., 2020; Lahaye & Robic, 2007).

Simulated gastrointestinal digestion did not affect the molecular weight of ulvan (Fig. 1a), and the polysaccharide was detected intact in the digested supernatant, indicating its resistance to gastric acid and digestive enzymes. This stability was further supported by ^{1}H NMR analysis of the digested samples (Fig. 1c), which, despite partial signal overlap caused by digestion reagents, showed no change in the relative proportion of the H6 signals of rhamnose (1.2–1.4 ppm), distinguishing free from bound forms (Chi et al., 2020); and indicating the absence of significant depolymerization. Additional signals appeared in the anomeric region (5.41; 5.23; and 4.45 ppm); however; these could not be attributed to the main monosaccharides present in ulvan. The signal at 5.41 ppm; previously attributed to xylose H1 (Zonfrillo, Bellumori, Digiglio, et al., 2025); was not confirmed in our subsequent work (Zonfrillo, Bellumori, Truzzi, et al., 2025). Although minor structural modifications induced by digestion cannot be completely excluded; the preservation of the characteristic ulvan NMR signals; together with GPC data confirm the resistance of ulvan to simulated digestion and support its classification as a soluble dietary fiber (Lahaye & Jegou, 1993; Liu et al., 2025).

During the subsequent colonic fermentation, the intensity of the chromatographic peak of ulvan decreased progressively, reaching a reduction of 20.20 ± 9.44% at the end of the fermentation (48 h), and suggesting that ulvan was utilized as substrate by gut microbiota (Fig. 1b).

3.2. Targeted analysis monitoring key microbial metabolites

3.2.1. pH changes

As a first indicator of microbial activity, pH was monitored over time. A decrease in pH reflects the production of SCFA and other acidic metabolites, indicating microbial fermentation (Procházková et al., 2024). The initial pH was approximately 7.0 and decreased progressively over time (Fig. 2a). The most pronounced decrease was observed for inulin, reaching a final pH of 5.0 after 48 h, while ulvan led to moderate acidification, comparable to that induced by the growth control.

Table 1
Constituent sugars, sulfate content and average molecular weight (Mw) of ulvan used for the *in vitro* fermentation.

Rha (mol%)	GlcA (mol%)	IdoA (mol%)	Xyl (mol%)	Glu (mol%)	Gal (mol%)	Total sugars (μg/mg)	SO_4^{2-} (%)	Mw (kDa)
51.27	20.28	7.41	6.36	12.99	1.38	612	16.61	88.36

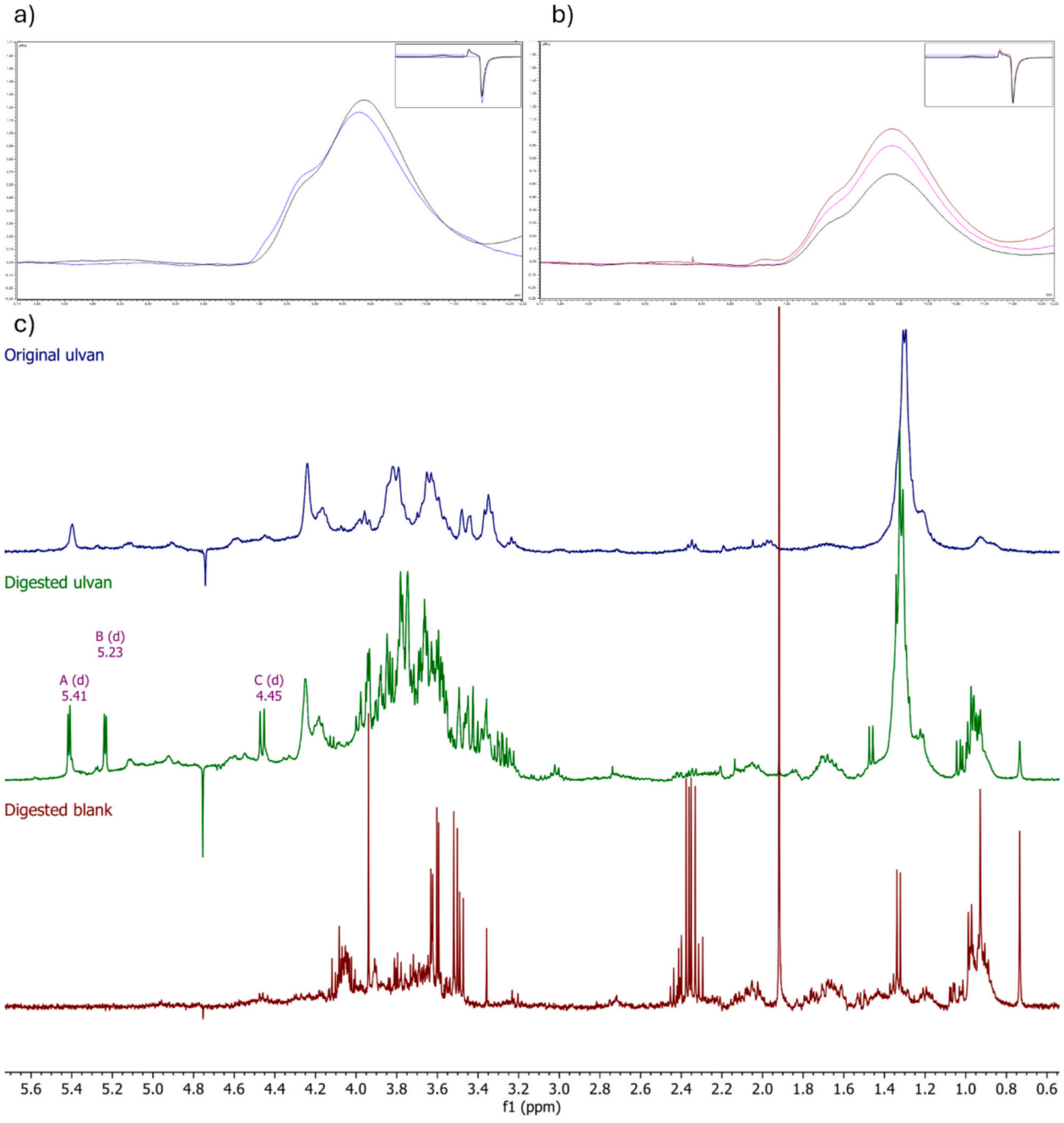

Fig. 1. a) HPGPC-RID chromatograms of original ulvan (blue) and ulvan after simulated digestion (black); **b)** HPGPC-RID chromatograms of fermented ulvan at 0 h (brown), 24 h (pink), and 48 h (black); **c)** ^{1}H NMR spectra of original ulvan (blue), and of the supernatants of digested ulvan (green) and digested blank (brown). (For interpretation of the references to colour in this figure legend, the reader is referred to the web version of this article.)

3.2.2. *Production of SCFA and BCFA*

SCFA, mainly acetic, propionic, and butyric acids, are the main catabolite of polysaccharide fermentation (Gill et al., 2021); while BCFA (isobutyric; valeric; and isovaleric acids) derive from amino acid catabolism and are markers of proteolytic fermentation (Gozdzik et al., 2023). Together, these metabolites provide insight into whether the microbiota is metabolizing carbohydrates or proteins under a given condition.

In this study, total SCFA levels increased over time across all treatments (Fig. 2b). Ulvan supplementation resulted in significantly higher SCFA levels than the growth control after 24 and 48 h, reaching levels statistically comparable to inulin, a well-established prebiotic fiber. Among the SCFA, acetic acid was the predominant product (Fig. S2), with ulvan and inulin yielding comparable production levels, both

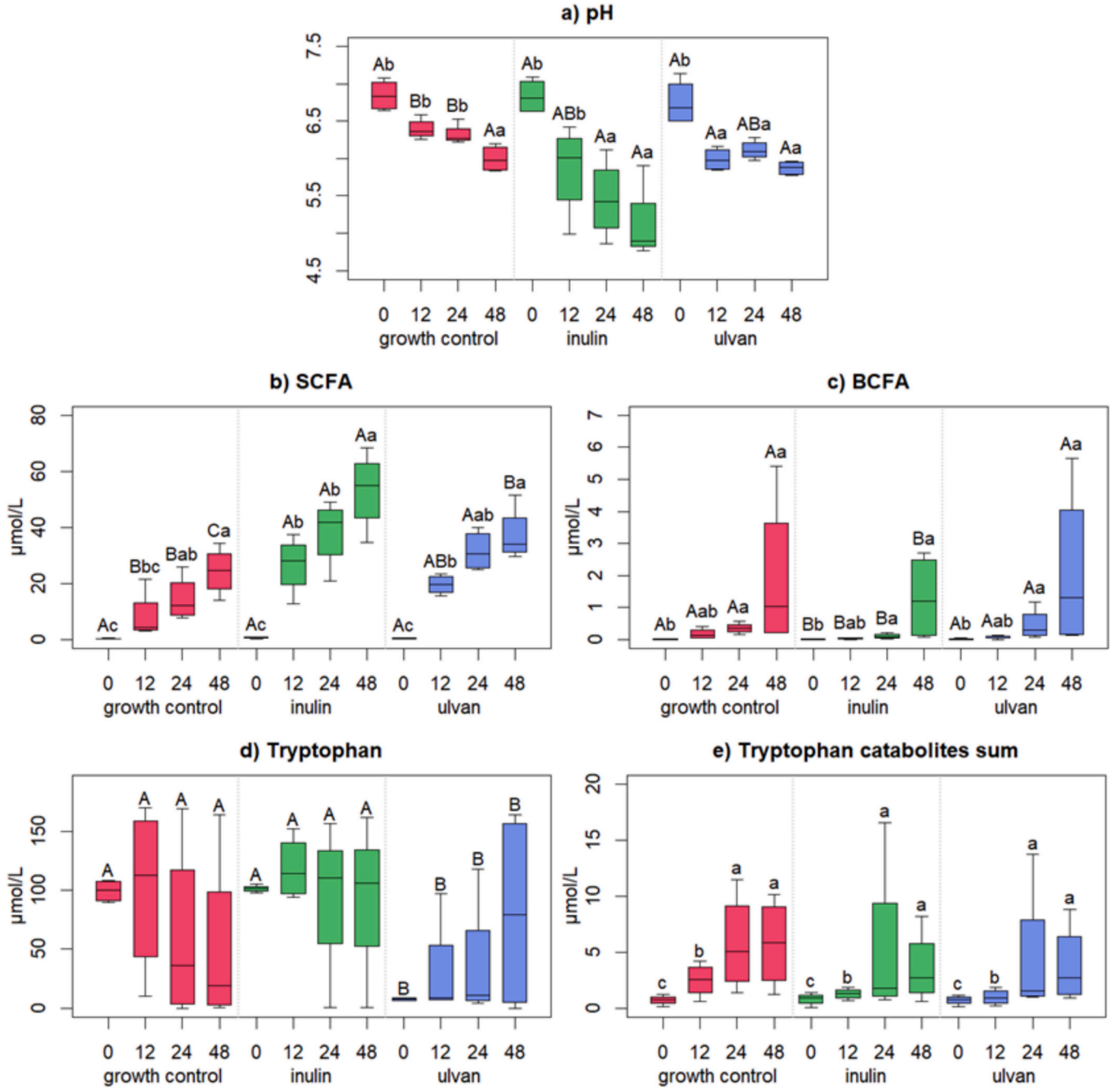

Fig. 2. Boxplots illustrating a) changes in pH, **b)** total SCFA (acetic, propionic, and butyric acids), c) total BCFA (isobutyric, isovaleric, and valeric acids), d) tryptophan and **e)** total tryptophan catabolites **production of growth control, inulin, and ulvan at different time points.** Significant differences over time points within each treatment and between treatments at the same time point are indicated by different lowercase and uppercase letters, respectively ($p < 0.05$).

significantly higher than the control.

BCFA concentrations gradually increased over time in all groups (Fig. 2c and Fig. S2), likely because of the protein fermentation of the medium. Ulvan samples showed BCFA levels similar to the control and consistently higher than inulin at all time points. Donor-specific differences were observed: donors 3 and 4 showed pronounced BCFA production, whereas donors 1 and 2 had only negligible amounts (data not shown). For inulin, donors 2 and 3 produced the highest BCFA amounts (data not shown). These observations confirm the influence of the initial composition of the fecal microbiota on the metabolic response to fiber supplementation (Dell'Olio et al., 2024; Murga-Garrido et al., 2021).

Our findings differ from early reports of limited SCFA production from ulvan fermentation (Durand et al., 1997; Kong et al., 2016), and supports the hypothesis that ulvan is indeed fermentable by human gut microbiota. The predominance of acetic acid is consistent with previous findings for both ulvan (Durand et al., 1997; Kong et al., 2016; Seong et al., 2019) and inulin (Gill et al., 2021). In the gut; acetic acid originates from the conversion of pyruvate; which is generated from simple sugars; released during microbial hydrolysis of polysaccharides; through glycolysis or the pentose phosphate pathway (Deleu et al., 2021). Acetate production is widespread among gut microbes and represents a central step for SCFA production; in fact; propionate and butyrate are synthesized through more specific pathways that often involve acetate as a precursor; and typically involve cross-feeding interactions (Deleu et al., 2021). In our study, acetic acid increased steadily during ulvan and inulin fermentations, suggesting that ulvan-derived sugars were

primarily directed into the acetate pathway without extensive conversion into other SCFA.

In the case of inulin, hydrolysis is mediated by β-fructofuranosidase enzymes expressed by *Bacteroidetes, Bifidobacteria,* and *Lactobacillus* species (Sonnenburg et al., 2010; Wilson & Whelan, 2017), whereas depolymerization and saccharolytic utilization of ulvan are predominantly driven by ulvan-specific CAZymes encoded by *Bacteroides spp.* (Gotteland et al., 2020). Despite its distinct structural features, we hypothesize that ulvan provides fermentable monosaccharides that feed into the central carbohydrate metabolism and converge on pyruvate, ultimately supporting acetic acid production comparable to that of inulin and potentially stimulating the growth of health-associated taxa.

To better visualize differences among treatments, RM-ASCA was applied to the targeted metabolite dataset. This multivariate model combines ANOVA with PCA and is useful to explain the temporal evolution of metabolites (Jarmund et al., 2022). PC1 (50.15% of variance) captured the general time-related fermentation process, as indicated by increasing scores across all treatments (Fig. 3A). PC2 (21.23%) well discriminated treatments over time, showing an initial score drop (0–24 h) followed by a marked increase (24–48 h) (Fig. 3C). PC3 (14.22%) separated polysaccharide-supplemented samples (ulvan and inulin, with negative scores) from the control (positive scores) (Fig. 3E). Importantly, SCFA (particularly acetic acid and propionic acid) were associated with negative loadings in PC3, indicating higher production in ulvan and inulin, whereas BCFA (especially isovaleric acid and isobutyric acid) had positive loadings, reflecting more pronounced proteolytic activity in the absence of polysaccharide supplementation. Collectively, these results indicate that ulvan undergoes saccharolytic fermentation, leading to high levels of acetate comparable to those of inulin. BCFA production did not differ significantly from the control in univariate analysis; however, multivariate modeling revealed higher contributions of BCFA in the control group, suggesting a shift toward proteolytic fermentation in the absence of polysaccharide supplementation. These findings therefore sustain the classification of ulvan as a fermentable polysaccharide.

3.2.3. Tryptophan catabolism

Tryptophan (Trp) is an essential amino acid metabolized in the gastrointestinal tract by both the host and gut microbiota, producing a variety of metabolites that influence host metabolism and homeostasis (Kim et al., 2024). The metabolic pathways of Trp known in the gastrointestinal tract are: (1) the serotonin (5-HT) pathway; (2) the kynurenine (Kyn) pathway; and (3) the indole (Ind) pathway (Agus et al., 2018). Recent findings highlighted that the production of specific tryptophan metabolites is more influenced by substrate-dependent regulation of specific metabolic pathways than by the abundance of tryptophan-metabolizing bacteria (Oba et al., 2020; Qi et al., 2022). In particular, fermentable fibers have been reported to stimulate the production of health-associated indole derivatives (Sinha et al., 2024).

In the present study, Trp concentrations were initially high in growth control and inulin samples – reflecting the presence of protein in the medium – and declined slightly over time (**Fig.** 2d), consistent with gradual microbial catabolism, as also suggested by the increasing trend of total Trp catabolites (Fig. 2e). In contrast, Trp levels in ulvan samples were almost zero at baseline but progressively increased during fermentation, although the trend did not reach statistical significance due to inter-donor variability. This atypical starting point suggests that ulvan may interact with medium proteins, transiently reducing the measurable Trp and releasing it as ulvan undergoes microbial depolymerization.

Analysis of the kynurenine pathway revealed that ulvan significantly increased Kyn concentrations compared with both inulin and control (Fig. S3), a result confirmed by its positive loading on PC2 (Fig. 3D). Although Kyn levels (median 0.14 μmol/L) remained within physiological ranges reported in other *in vitro* fermentation studies (Huang, Boekhorst, et al., 2023; Huang, De Vries, et al., 2023), Kyn mediates a critical pathway linked to immune modulation (Agus et al., 2018).

A more pronounced effect of ulvan was observed on the indole pathway. During the last 24 h of fermentation, ulvan showed the steepest increase in PC2 scores (Fig. 3C), linked to significant rises in indole-3-propionic acid (IPA) and indole-3-acetic acid (IAA), whereas indole-3-lactic acid (ILA) decreased (Fig. 3D). In ulvan samples, IAA concentrations were higher than those of the two controls during the entire fermentation (Fig. S3), while ILA levels increased in the first 24 h of fermentation and declined thereafter, coinciding with the rise in IPA levels (Fig. S3). For inulin, this trend was not observed, as ILA levels rose progressively while IPA remained low.

These findings are in line with recent *in vitro* and *in vivo* studies, which demonstrate that dietary fibers, such as pectin, promote the production of IPA and IAA (Dell'Olio et al., 2024; Huang, De Vries, et al., 2023). The sequential pattern of ILA and IPA supports the hypothesis of a cross-feeding mechanism, where ILA, produced by primary fermenters (*e.g.*, *Bacteroides*, *Bifidobacterium,* and *Lactobacillus*), is further converted to IPA and IAA by secondary species such as *Clostridium sporogenes*, as demonstrated before (Roager & Licht, 2018; Wang et al., 2024). Functionally, these metabolites are relevant because ILA and IAA are aryl hydrocarbon receptor (AhR) ligands involved in maintaining intestinal homeostasis through modulation of epithelial integrity and immune cell function (Lamas et al., 2018). ILA; in particular; has been associated with the regulation of Treg/Th17 cell balance; a key mechanism in autoimmune and inflammatory diseases (Roager & Licht, 2018); while IAA attenuates pro-inflammatory cytokine responses (Roager & Licht, 2018). IPA acts as a pregnane X receptor (PXR) agonist; contributing to intestinal barrier protection; and has been inversely associated with type-2 diabetes risk in a human cohort study (Huang et al., 2024; Lamas et al., 2016; Qi et al., 2022). The subsequent IPA production following early ILA accumulation suggests that ulvan may promote the activity of primary saccharolytic fermenters, thereby initiating Trp catabolism, and supporting metabolic cross-feeding that enhances the synthesis of secondary indole derivatives. Thus, ulvan appears to modulate gut metabolism not only by providing a fermentable carbon source but also by shaping Trp catabolism toward the production of AhR- and PXR agonists with potential beneficial effects on gut homeostasis.

Tryptamine (TA), a decarboxylation product of Trp and a precursor of 5-HT, showed the highest negative loading in PC2 and positive loading in PC3 (Fig. 3D and F), indicating that its production was reduced in fiber-supplemented groups, particularly in ulvan samples (Fig. S3). This reduction has also been observed in SHIME models with inulin and pectin (Huang, Boekhorst, et al., 2023) and likely reflects a redirection of Trp metabolism under saccharolytic conditions.

Finally, Ind was the most abundant metabolite across all treatments (Fig. S3), consistent with previous studies (Roager & Licht, 2018); but showed relatively lower accumulation in ulvan and inulin samples; as confirmed by its positive loading on PC3 (Fig. 3F). This reduction may result from catabolite repression; whereby monosaccharides released during fiber degradation suppress the expression of genes involved in the metabolism of other compounds (Stülke & Hillen, 1999). Previous studies have shown how pectin; degraded by *Bacteroides thetaiotaomicron*; suppressed the expression of indole-producing genes in *E. coli*; redirecting the available Trp toward the production of ILA and IPA by other species such as *C. sporogenes* (Sinha et al., 2024).

Taken together, these results indicate that ulvan not only undergoes saccharolytic fermentation but also modulates Trp catabolism by favoring the production of anti-inflammatory and barrier-supporting metabolites (IPA, IAA, ILA) and reducing the accumulation of TA and Ind. Although microbiota composition was not analyzed in this study, precluding direct confirmation of specific microbial interactions, the temporal association between ILA and IPA points to cross-feeding interactions similar to those reported for other complex polysaccharides. Possibly, *Bacteroides* species mediated ulvan degradation (Liu et al., 2025) releasing substrates that, in turn, are converted into health-promoting indole derivatives. Therefore, this highlights ulvan's

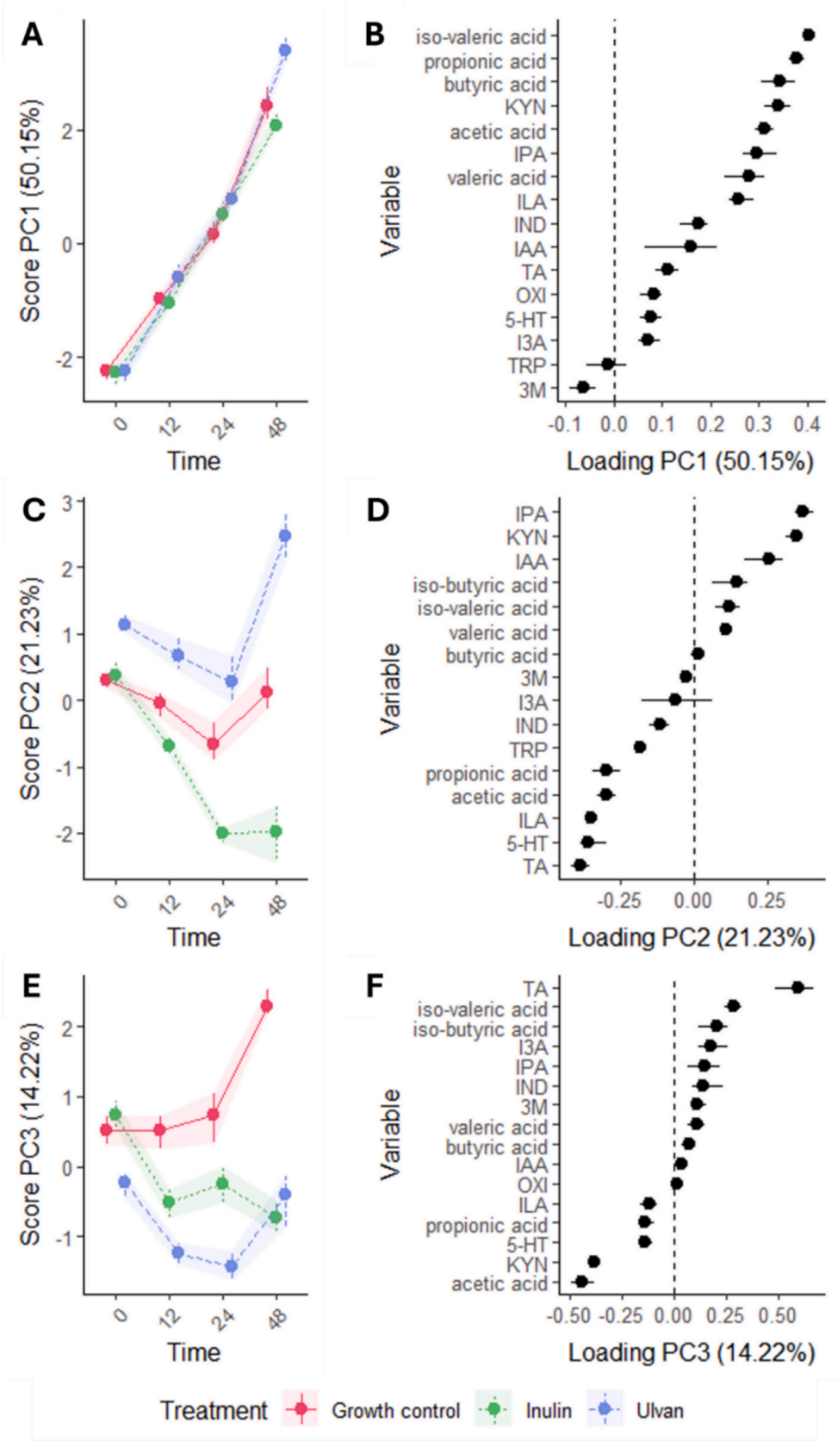

Fig. 3. RM-ASCA model explaining the temporal evolution of SCFA and tryptophan metabolites during 48 h of fermentation in growth control (red), inulin (green), and ulvan (blue) treatments. The score plots (Fig. 3 panels A, C, and E) display the trends of the principal component scores (PC1, PC2, and PC3), which explain 50.15%, 21.23%, and 14.22% of the total variance, respectively. Each principal component represents a direction of variability in the data, allowing discrimination of treatment- and time-related effects (Jarmund et al., 2022). The corresponding loading plots (Fig. 3, panels B, D, and F) illustrate the metabolites contributing positively or negatively to each component. Increases in component scores correspond to increases in metabolites with positive loadings and decreases in those with negative loadings, and *vice versa*. Error bars and shaded areas represent 95% confidence intervals calculated using jack-knife validation ($n = 1000$). (For interpretation of the references to colour in this figure legend, the reader is referred to the web version of this article.)

potential as a prebiotic.

3.3. Untargeted data

Untargeted metabolomics was employed to obtain a comprehensive overview of the metabolic transformations occurring during ulvan fermentation, beyond SCFA and Trp-derived metabolites. This approach enabled us to investigate whether ulvan, compared with inulin and the control, induces distinct metabolic patterns and to identify additional metabolite classes potentially associated with its microbial degradation. Samples were acquired by LC-HRMS in both positive (ESI+) and negative (ESI−) ionization modes and processed independently following the workflow shown in Fig. S1. The quality of the data was confirmed by PCA of the aligned features, which showed clustering of QC pools (Fig. S4). After annotation and filtering (Section 2.10), 943 features (126 with MSI level 2a) for ESI+ and 485 features (47 with level 2a) for ESI− were retained for analysis. Multivariate analysis using PLS-DA clearly separated treatments (Fig. 4), suggesting that ulvan fermentation induced a distinct metabolome compared to control and inulin.

To capture temporal dynamics, RM-ASCA models were built separately for ESI+ and ESI- datasets (Fig. 5). In both cases, PC1 explained most of the variance (66.22% for ESI+, 72.00% for ESI−) and reflected the global fermentation process, with scores decreasing over time across all treatments (Fig. 5A). Features with high positive loadings on PC1 included peptides and bile acids, indicating protein degradation and bile acid transformation. In contrast, negatively loaded features were mostly fatty acid derivatives, which increased during fermentation (Table S2). PC2 (12.05% for ESI+ and 7.29% for ESI-) captured treatment-specific effects, differentiating between ulvan and inulin, as well as the control, in both datasets (Fig. 5B). PC3 (6.44% for ESI+, and 6.12% for ESI-) further distinguished carbohydrate-supplemented samples (ulvan and inulin) from the control, with positive loadings associated with metabolites enriched in fiber-supplemented conditions (Fig. 5C). PC2 and PC3 scores (from ESI- dataset) followed a similar time course, initially increasing (0−12h) and then decreasing, suggesting the release of intermediate metabolites, such as small peptides or oligosaccharides derived from protein or carbohydrate degradation, by ulvan, followed by their subsequent degradation.

Table 2 summarizes the most discriminant features associated with PC2 and PC3 for both datasets, selected from the 24 features with the highest loadings in each component (see individual temporal plots in Figs. S5 and S6). Three metabolites were annotated with MSI confidence level 2a and further investigated using microbeMASST, tentatively linking their MS/MS spectra to possible microbial producers (Zuffa et al., 2024). Among them; two proline dipeptides showed opposite trends: cyclo-(Pro-Pro) decreased; whereas cyclo-(Pro-Met) increased in ulvan samples. These peptides have been associated with *Bacteroides; Ligilactobacillus; Bifidobacterium;* and *Lactobacillus* species (Fig. S7). Certain *Lactobacillus* species are known to exhibit peptidase activity; specifically on proline peptides; as they express high levels of proline dipeptidase (Brzozowski et al., 2009; Luoma et al., 2001; Morel et al., 1999; Tamime & Robinson, 2007). Thus, the association of proline dipeptides with lactic acid bacteria, such as *Lactobacillus* species, may indicate that ulvan either promotes their abundance or induces proline dipeptidase expression, supporting its prebiotic potential. Proline dipeptides have been linked to diverse bioactivities, including glycosidase inhibition, antimicrobial properties, and quorum-sensing signaling (Axel et al., 2014). Moreover, the opposite trends in cyclo-(Pro-Pro) and cyclo-(Pro-Met) may indicate functional remodeling of proteolytic activity, possibly linked to changes in microbial expression or community structure, particularly involving lactic acid bacteria. We also detected a significant decrease in the oligopeptide Ac-Asp-Asp-Ile-Val-Pro-amBA-OH in ulvan samples, suggesting microbial degradation, although no microbial producers were identified *via* microbeMASST.

RM-ASCA models further identified features that could provide insights into ulvan's metabolic fate. Decreasing features included an oligopeptide (*m/z*_Rt 707.32294_6.84) and a depsipeptide (*m/z*_Rt 746.35663_7.34), both detected exclusively in ulvan samples and likely originating from ulvan-protein complexes degraded during fermentation. Conversely, several features increased during fermentation and may represent degradation products or ulvan-specific metabolites, some of which contained sulfur (the S-alkyl thiosulfate 230.9462_2.69, the biotin derivative 815.39158_6.55, the benzenoid 414.88465_1.09, the oligopeptide 400.00456_1.11, and the arylsulfonic acid 573.14536_1.46). To our knowledge, these features have not been reported in other studies, which limits further interpretation but suggests they may serve as markers of ulvan fermentation.

To further integrate targeted and untargeted metabolomics, a

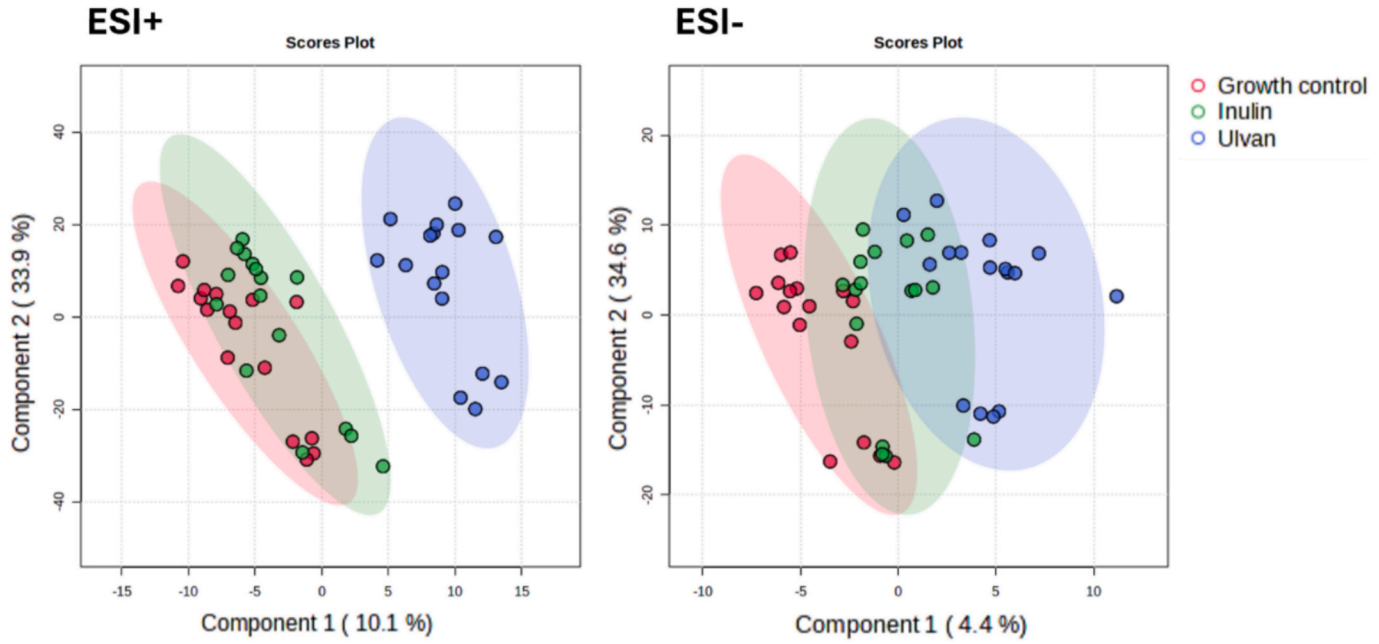

Fig. 4. Principal Least Squares-Discriminant Analysis (PLS-DA) scores plots of growth control (red), inulin (green), and ulvan (blue) of positive (ESI+) and negative (ESI-) datasets. (For interpretation of the references to colour in this figure legend, the reader is referred to the web version of this article.)

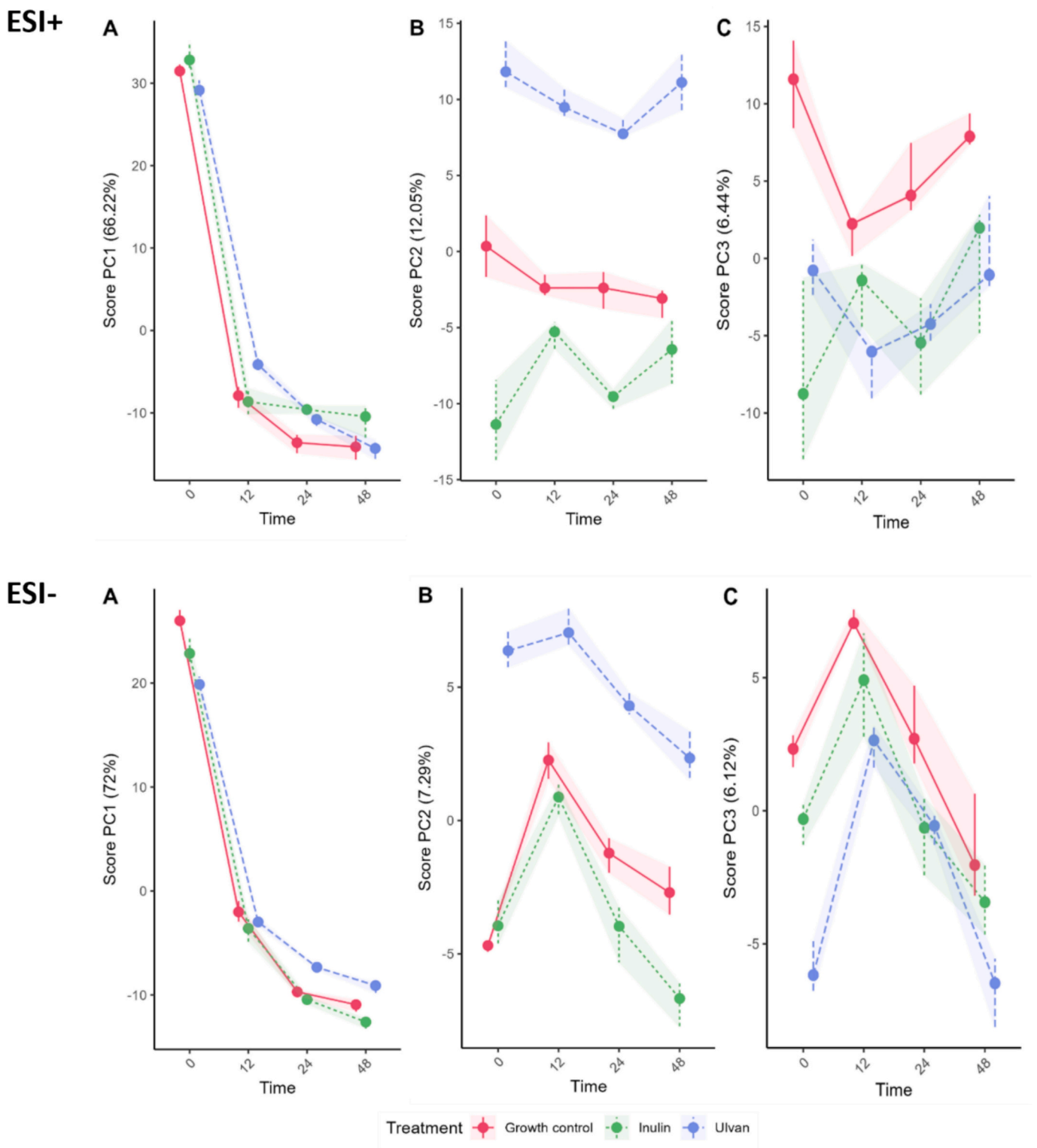

Fig. 5. RM-ASCA model explaining the temporal evolution of features detected in positive (ESI+) and negative (ESI-) ionization modes during 48 h of fermentation in growth control (red), inulin (green), and ulvan (blue) treatments. The score plots show the trends of the principal component scores PC1 (A), PC2 (B), and PC3 (C). Error bars and shaded areas represent 95% confidence intervals calculated using jack-knife validation ($n = 1000$). (For interpretation of the references to colour in this figure legend, the reader is referred to the web version of this article.)

combined RM-ASCA model was built using the full dataset. The integrated analysis confirmed the main temporal and treatment-related trends observed in the separate models, with PC1 capturing the global fermentation process, PC2 distinguishing ulvan from inulin and the control, and PC3 separating fiber-supplemented from non-supplemented conditions (Fig. S8). Examination of the 48 features with the highest positive and negative loadings on PC2 and PC3 confirmed the metabolites previously associated with treatment-specific effects (Table 2). Most discriminant variables belonged to the untargeted datasets, while only kynurenine (PC2) and isovaleric acid (PC3) from the targeted

Table 2
Significant features detected in ulvan fermented samples. The table reports the "*m/z*_Rt" in accordance with Figs. S5 and S6, the loading and its associated PC and trend over time (↗ increasing, ↘ decreasing, ↔ steady), molecular formula, MSI confidence level of identification, name, classification, and ionization.

*m/z*_Rt	PC	loading	Trend	Molecular Formula	MSI confidence level	Name	Classification	ESI
229.10056_5.16	2	0.08	↗	$C_{10}H_{16}N_2O_2S$	level 2a	cyclo-(Pro-Met)	Dipeptide	+
195.11298_3.06	2	0.10	↘	$C_{10}H_{14}N_2O_2$	level 2a	cyclo-(Pro-Pro)	Dipeptides	+
685.34023_6.91	2 3	0.10 −0.06	↘	$C_{30}H_{48}N_6O_{12}$	level 2a	Ac-Asp-Asp-Ile-Val-Pro-amBA-OH	Oligopeptide	+
515.28513_7.37	2	0.12	↘	$C_{26}H_{44}O_{10}$	level 3		Diterpenoids	−
214.00215_1.06	2 3	0.10 −0.07	↔	$C_{10}H_7O_3$	level 3		1-hydroxy-2-unsubstituted benzenoides	+
707.32294_6.84	2 3	0.10 −0.06	↘	$C_{30}H_{48}N_6O_{12}$	level 3		Oligopeptides	+
746.35663_7.34	2	0.08	↘	$C_{38}H_{53}N_5O_8$	level 3		Depsipeptides	+
135.03115_1.09	2	0.09	↗	$C_5H_4N_4O$	level 3		Purine alkaloids	−
230.9462_2.69	3	−0.08	↗	$C_4H_8O_5S_3$	level 3		S-alkyl thiosulfates	−
267.11902_2.05	4	−0.06	↗	$C_{10}H_{14}N_6O_3$	level 3		Purine nucleos(*t*)ides	+
282.13234_10.46	3	−0.07	↗	$C_{10}H_{17}N_7O_3$	level 3		Small peptides	−
302.10088_9.4	3	−0.08	↗	$C_{12}H_{13}N_7O_3$	level 3		Pseudoalkaloids	−
400.00456_1.11	2	0.10	↗	$C_{12}H_{15}N_3O_6S_2$	level 3		Oligopeptide	+
414.88465_1.09	3 4	−0.04 −0.05	↗	$C_{15}H_6O_3P_2S_3$	level 3		Benzenoids	+
434.85453_1.05	2 3	0.10 −0.09	↗	$C_{10}H_6N_2O_8Se$	level 4		/	−
780.45883_8.4	2	0.09	↗	$C_{36}H_{58}N_8O_{10}$	level 3		Oligopeptides	+
824.48512_8.62	2	0.10	↗	$C_{40}H_{58}N_{10}O_8$	level 3		Peptides	+
344.9709_3.28	2	0.09	↗↘	$C_8H_{14}N_2O_5S_4$	level 3		Dipeptides	−
573.14536_1.46	3	−0.05	↗↔	$C_{29}H_{24}N_4O_7S$	level 3		Arylsulfonic acids and derivatives	+
815.39158_6.55	2 3	0.11 −0.06	↔	$C_{45}H_{58}N_4O_6S_2$	level 3		Biotin and derivatives	+
868.51063_8.81	2	0.10	↔	$C_{40}H_{66}N_8O_{12}$	level 3		Oligopeptides	+

dataset ranked among the top contributors (data not shown). The overlap between discriminant features and those identified in the individual analyses supports the complementarity of the two approaches and indicates that untargeted metabolomics captured additional metabolic information beyond classical fermentation markers, while remaining coherent with the targeted results.

Overall, the untargeted metabolomics approach provided novel insights into the metabolic profile associated with ulvan fermentation. The most informative results came from cyclic proline dipeptides, which suggested selective stimulation of beneficial microbial groups and thus support a potential prebiotic effect. Other features, including peptides, fatty acid derivatives, sulfur-containing compounds, and putative ulvan-protein conjugates, showed distinct abundance patterns in ulvan samples but remain largely unknown. This underscores the need for further structural and functional characterization. Together with targeted SCFA and tryptophan metabolite data, these results indicate that ulvan promotes gradual microbial degradation and the production of bioactive microbial metabolites, supporting the hypothesis of fiber-driven cross-feeding interactions.

These results should be interpreted in consideration of some limitations. First, the *in vitro* model of gastrointestinal digestion and colonic fermentation, although standardized, cannot fully capture *in vivo* complexity, including host-microbe interactions, immune signaling, and metabolite absorption. Second, the observed metabolic responses should be regarded as functional outcomes under controlled experimental conditions rather than direct predictors of *in vivo* effects. Third, the absence of microbiota sequencing prevents direct identification of the taxa responsible for ulvan degradation and metabolite production, precluding direct validation of the proposed cross-feeding mechanisms. Four, many untargeted features remain at MSI level 3, and the lack of comprehensive reference libraries for microbial metabolites limits confident annotation. Despite these limitations, this study offers one of the first comprehensive metabolomic characterizations of ulvan fermentation, providing unique insights into its metabolic fate and suggesting a potential prebiotic effect.

4. Conclusion

This study provides novel and comprehensive insights into the fermentability and metabolic effects of ulvan, a sulfated polysaccharide extracted from *U. lactuca* L., using an *in vitro* colonic fermentation model. Our results demonstrate that ulvan acts as a fermentable dietary fiber, resisting gastrointestinal digestion and reaching the colon intact, where it can be metabolized by the gut microbiota. The combined evidence from targeted and untargeted metabolomics supports the hypothesis that ulvan possesses a prebiotic capacity. In particular, ulvan stimulated SCFA production, primarily acetic acid, at levels comparable to those of the established prebiotic inulin. Moreover, it selectively modulated microbial tryptophan metabolism, enhancing the production of bioactive metabolites such as indole-3-propionic acid and indole-3-acetic acid, which are associated with intestinal barrier protection and immune regulation. This microbial metabolite production supports the hypothesis that fiber-driven cross-feeding mechanisms previously described for tryptophan metabolism. In particular, the sequential dynamics of these metabolites, together with the reduced accumulation of tryptamine and indole under fiber-supplemented conditions, suggest a shift in microbial tryptophan catabolism toward the production of bioactive indole derivatives. However, confirmation of the microbial taxa involved require complementary microbiome analyses such as shotgun metagenomics. Untargeted metabolomics further revealed distinct shifts in the colonic metabolome, including potential ulvan-specific metabolites, providing new candidate biomarkers of ulvan utilization.

Overall, this study provides one of the first detailed metabolic characterizations of ulvan fermentation, showing that ulvan not only stimulates saccharolytic activity but also modulates amino acid catabolism and microbial metabolic functions, generating testable hypotheses for future *in vivo* and multi-omics studies to confirm its microbiota-mediated mechanisms and health relevance. These findings highlight ulvan's potential as a functional food ingredient for promoting gut health, opening new perspectives for the valorization of *Ulva* biomass in nutrition and human health applications.

CRediT authorship contribution statement

Beatrice Zonfrillo: Writing – original draft, Methodology, Investigation, Formal analysis, Data curation, Conceptualization. **Carmen M.S. Ambrosio:** Writing – review & editing, Supervision, Investigation, Conceptualization. **Nadia Mulinacci:** Writing – review & editing, Supervision, Resources, Funding acquisition, Conceptualization. **Josep Rubert:** Writing – review & editing, Supervision, Resources, Methodology, Conceptualization.

Declaration of competing interest

The authors declare that they have no known competing financial interests or personal relationships that could have appeared to influence the work reported in this paper.

Acknowledgements

The Food Quality and Design chair group at Wageningen University supported this research using internal funding. The graphical abstract was created in BioRender. Zonfrillo, B. (2025) https://BioRender.com/pzpggli

Appendix A. Supplementary data

Supplementary data to this article can be found online at https://doi.org/10.1016/j.foodchem.2026.149100.

Data availability

Data will be made available on request.

References

Agus, A., Planchais, J., & Sokol, H. (2018). Gut microbiota regulation of tryptophan metabolism in health and disease. *Cell Host & Microbe, 23*(6), 716–724. https://doi.org/10.1016/j.chom.2018.05.003

Araújo, R., & Peteiro, C. (2021). *Algae as food and food supplements in Europe*. JRC Publications Repository. https://doi.org/10.2760/049515

Ardizzone, A., Mannino, D., Capra, A. P., Repici, A., Filippone, A., Esposito, E., & Campolo, M. (2023). New insights into the mechanism of *ulva pertusa* on colitis in mice: Modulation of the pain and immune system. *Marine Drugs, 21*(5), Article 298. https://doi.org/10.3390/md21050298

Axel, C., Zannini, E., Arendt, E. K., Waters, D. M., & Czerny, M. (2014). Quantification of cyclic dipeptides from cultures of lactobacillus brevis R2Δ by HRGC/MS using stable isotope dilution assay. *Analytical and Bioanalytical Chemistry, 406*(9), 2433–2444. https://doi.org/10.1007/s00216-014-7620-3

Beer, S. (2023). Photosynthetic traits of the ubiquitous and prolific macroalga ulva (chlorophyta): A review. *European Journal of Phycology, 58*(4), 390–398. https://doi.org/10.1080/09670262.2022.2150894

Brodkorb, A., Egger, L., Alminger, M., Alvito, P., Assunção, R., Ballance, S., Bohn, T., Bourlieu-Lacanal, C., Boutrou, R., Carrière, F., Clemente, A., Corredig, M., Dupont, D., Dufour, C., Edwards, C., Golding, M., Karakaya, S., Kirkhus, B., Le Feunteun, S., … Recio, I. (2019). INFOGEST static in vitro simulation of gastrointestinal food digestion. *Nature Protocols, 14*(4), 991–1014. https://doi.org/10.1038/s41596-018-0119-1

Brzozowski, B., Bednarski, W., & Dziuba, B. (2009). Functional properties of *lactobacillus acidophilus* metabolites. *Journal of the Science of Food and Agriculture, 89*(14), 2467–2476. https://doi.org/10.1002/jsfa.3749

Chambers, M. C., Maclean, B., Burke, R., Amodei, D., Ruderman, D. L., Neumann, S., … Mallick, P. (2012). A cross-platform toolkit for mass spectrometry and proteomics. *Nature Biotechnology, 30*(10), 918–920. https://doi.org/10.1038/nbt.2377

Charoensiddhi, S., Conlon, M., Methacanon, P., Thayanukul, P., Hongsprabhas, P., & Zhang, W. (2022). Gut microbiome modulation and gastrointestinal digestibility *in vitro* of polysaccharide-enriched extracts and seaweeds from *ulva rigida* and *gracilaria fisheri*. *Journal of Functional Foods, 96*, Article 105204. https://doi.org/10.1016/j.jff.2022.105204

Cherry, P., Yadav, S., Strain, C. R., Allsopp, P. J., McSorley, E. M., Ross, R. P., & Stanton, C. (2019). Prebiotics from seaweeds: An ocean of opportunity? *Marine Drugs, 17*(6), Article 327. https://doi.org/10.3390/md17060327

Chi, Y., Li, H., Wang, P., Du, C., Ye, H., Zuo, S., Guan, H., & Wang, P. (2020). Structural characterization of ulvan extracted from *ulva* clathrata assisted by an ulvan lyase. *Carbohydrate Polymers, 229*, Article 115497. https://doi.org/10.1016/j.carbpol.2019.115497

De Ruiter, G. A., Schols, H. A., Voragen, A. G. J., & Rombouts, F. M. (1992). Carbohydrate analysis of water-soluble uronic acid-containing polysaccharides with high-performance anion-exchange chromatography using methanolysis combined with TFA hydrolysis is superior to four other methods. *Analytical Biochemistry, 207*(1), 176–185. https://doi.org/10.1016/0003-2697(92)90520-H

Deleu, S., Machiels, K., Raes, J., Verbeke, K., & Vermeire, S. (2021). Short chain fatty acids and its producing organisms: An overlooked therapy for IBD? *EBioMedicine, 66*. https://doi.org/10.1016/j.ebiom.2021.103293

Dell'Olio, A., Scott, W. T., Taroncher-Ferrer, S., San Onofre, N., Soriano, J. M., & Rubert, J. (2024). Tailored impact of dietary fibers on gut microbiota: A multi-omics comparison on the lean and obese microbial communities. *Microbiome, 12*(1). https://doi.org/10.1186/s40168-024-01975-x

Dührkop, K., Fleischauer, M., Ludwig, M., Aksenov, A. A., Melnik, A. V., Meusel, M., … Böcker, S. (2019). SIRIUS 4: A rapid tool for turning tandem mass spectra into metabolite structure information. *Nature Methods, 16*(4), 299–302. https://doi.org/10.1038/s41592-019-0344-8

Dührkop, K., Nothias, L.-F., Fleischauer, M., Reher, R., Ludwig, M., Hoffmann, M. A., … Böcker, S. (2021). Systematic classification of unknown metabolites using high-resolution fragmentation mass spectra. *Nature Biotechnology, 39*(4), 462–471. https://doi.org/10.1038/s41587-020-0740-8

Dührkop, K., Shen, H., Meusel, M., Rousu, J., & Böcker, S. (2015). Searching molecular structure databases with tandem mass spectra using CSI: FingerID. *Proceedings of the National Academy of Sciences, 112*(41), 12580–12585. https://doi.org/10.1073/pnas.1509788112

Durand, M., Beaumatin, P., Bulman, B., Bemalier, A., Grivet, J., Serezat, M., Gramet, G., & Lahaye, M. (1997). Fermentation of green alga sea-lettuce (ulva sp) and metabolism of its sulphate by human colonic microbiota in a semi-continuous culture system. *Reproduction Nutrition Development, 37*(3), 267–283. https://doi.org/10.1051/rnd:19970303

Elkin, L. A., Kay, M., Higgins, J. J., & Wobbrock, J. O. (2021). *An aligned rank transform procedure for multifactor contrast tests. The 34th annual ACM symposium on user interface software and technology, UIST. 21* pp. 754–768). https://doi.org/10.1145/3472749.3474784

Gibson, G. R., Hutkins, R., Sanders, M. E., Prescott, S. L., Reimer, R. A., Salminen, S. J., … Reid, G. (2017). Expert consensus document: The international scientific association for probiotics and prebiotics (ISAPP) consensus statement on the definition and scope of prebiotics. *Nature Reviews Gastroenterology & Hepatology, 14*(8), 491–502. https://doi.org/10.1038/nrgastro.2017.75

Gill, S. K., Rossi, M., Bajka, B., & Whelan, K. (2021). Dietary fibre in gastrointestinal health and disease. *Nature Reviews Gastroenterology & Hepatology, 18*(2), 101–116. https://doi.org/10.1038/s41575-020-00375-4

González-Domínguez, Á., Estanyol-Torres, N., Brunius, C., Landberg, R., & González-Domínguez, R. (2024). QC omics: Recommendations and guidelines for robust, easily implementable and reportable quality control of metabolomics data. *Analytical Chemistry, 96*(3), 1064–1072. https://doi.org/10.1021/acs.analchem.3c03660

Gotteland, M., Riveros, K., Gasaly, N., Carcamo, C., Magne, F., Liabeuf, G., Beattie, A., & Rosenfeld, S. (2020). The pros and cons of using algal polysaccharides as prebiotics. *Frontiers in Nutrition, 7*, Article 163. https://doi.org/10.3389/fnut.2020.00163

Gozdzik, P., Magkos, F., Sledzinski, T., & Mika, A. (2023). Monomethyl branched-chain fatty acids: Health effects and biological mechanisms. *Progress in Lipid Research, 90*, Article 101226. https://doi.org/10.1016/j.plipres.2023.101226

Hoffmann, M. A., Nothias, L.-F., Ludwig, M., Fleischauer, M., Gentry, E. C., Witting, M., … Böcker, S. (2022). High-confidence structural annotation of metabolites absent from spectral libraries. *Nature Biotechnology, 40*(3), 411–421. https://doi.org/10.1038/s41587-021-01045-9

Holscher, H. D. (2017). Dietary fiber and prebiotics and the gastrointestinal microbiota. *Gut Microbes, 8*(2), 172–184. https://doi.org/10.1080/19490976.2017.1290756

Huang, Z., Boekhorst, J., Fogliano, V., Capuano, E., & Wells, J. M. (2023). Distinct effects of fiber and colon segment on microbiota-derived indoles and short-chain fatty acids. *Food Chemistry, 398*, Article 133801. https://doi.org/10.1016/j.foodchem.2022.133801

Huang, Z., De Vries, S., Fogliano, V., Wells, J. M., Van Der Wielen, N., & Capuano, E. (2023). Effect of whole foods on the microbial production of tryptophan-derived aryl hydrocarbon receptor agonists in growing pigs. *Food Chemistry, 416*, Article 135804. https://doi.org/10.1016/j.foodchem.2023.135804

Huang, Z., Wells, J. M., Fogliano, V., & Capuano, E. (2024). Microbial tryptophan catabolism as an actionable target via diet-microbiome interactions. *Critical Reviews in Food Science and Nutrition*, 1–15. https://doi.org/10.1080/10408398.2024.2369947

Izquierdo-Sandoval, D., Duan, X., Fryganas, C., Portolés, T., Sancho, J. V., & Rubert, J. (2024). Untargeted metabolomics unravels distinct gut microbial metabolites derived from plant-based and animal-origin proteins using in vitro modeling. *Food Chemistry, 457*, Article 140161. https://doi.org/10.1016/j.foodchem.2024.140161

Jarmund, A. H., Madssen, T. S., & Giskeødegård, G. F. (2022). ALASCA: An r package for longitudinal and cross-sectional analysis of multivariate data by ASCA-based methods. *Frontiers in Molecular Biosciences, 9*, Article 962431. https://doi.org/10.3389/fmolb.2022.962431

Kansandee, W., Moonmangmee, S., Vangpikul, S., Kosawatpat, P., & Tamtin, M. (2024). Physicochemical properties and in vitro prebiotic activity of *Ulva rigida* polysaccharides. *Biocatalysis and Agricultural Biotechnology, 59*, Article 103252. https://doi.org/10.1016/j.bcab.2024.103252

Kay, M., Elkin, L. A., Higgins, J. J., & Wobbrock, J. O. (2021). *Mjskay/ARTool: ARTool 0.11.0 (version v0.11.0) [computer software]. Zenodo. Doi;10.5281/zenodo.4721941*.

Kidgell, J. T., Magnusson, M., De Nys, R., & Glasson, C. R. K. (2019). Ulvan: A systematic review of extraction, composition and function. *Algal Research, 39*, Article 101422. https://doi.org/10.1016/j.algal.2019.101422

Kim, S., Seo, S.-U., & Kweon, M.-N. (2024). Gut microbiota-derived metabolites tune host homeostasis fate. *Seminars in Immunopathology, 46*(1–2), 2. https://doi.org/10.1007/s00281-024-01012-x

Kong, Q., Dong, S., Gao, J., & Jiang, C. (2016). In vitro fermentation of sulfated polysaccharides from *E. prolifera* and *L. japonica* by human fecal microbiota. *International Journal of Biological Macromolecules, 91*, 867–871. https://doi.org/10.1016/j.ijbiomac.2016.06.036

Lahaye, M., & Jegou, D. (1993). Chemical and physical-chemical characteristics of dietary fibres from *Ulva lactuca* (L.) thuret and *Enteromorpha compressa* (L.) grev. *Journal of Applied Phycology, 5*(2), Article 195. https://doi.org/10.1007/BF00004017

Lahaye, M., & Robic, A. (2007). Structure and functional properties of ulvan, a polysaccharide from green seaweeds. *Biomacromolecules, 8*(6), 1765–1774. https://doi.org/10.1021/bm061185q

Lamas, B., Natividad, J. M., & Sokol, H. (2018). Aryl hydrocarbon receptor and intestinal immunity. *Mucosal Immunology, 11*(4), 1024–1038. https://doi.org/10.1038/s41385-018-0019-2

Lamas, B., Richard, M. L., Leducq, V., Pham, H.-P., Michel, M.-L., Da Costa, G., … Sokol, H. (2016). CARD9 impacts colitis by altering gut microbiota metabolism of tryptophan into aryl hydrocarbon receptor ligands. *Nature Medicine, 22*(6), 598–605. https://doi.org/10.1038/nm.4102

Liu, Z., Wang, M., Li, J., Guo, X., Guo, Q., & Zhu, B. (2025). Differences in utilization and metabolism of ulva lactuca polysaccharide by human gut bacteroides species in the in vitro fermentation. *Carbohydrate Polymers, 351*, Article 123126. https://doi.org/10.1016/j.carbpol.2024.123126

Ludwig, M., Nothias, L.-F., Dührkop, K., Koester, I., Fleischauer, M., Hoffmann, M. A., … Böcker, S. (2020). Database-independent molecular formula annotation using gibbs sampling through ZODIAC. *Nature Machine Intelligence, 2*(10), 629–641. https://doi.org/10.1038/s42256-020-00234-6

Luoma, S., Peltoniemi, K., Joutsjoki, V., Rantanen, T., Tamminen, M., Heikkinen, I., & Palva, A. (2001). Expression of six peptidases fromLactobacillus helveticus in lactococcus lactis. *Applied and Environmental Microbiology, 67*(3), 1232–1238. https://doi.org/10.1128/AEM.67.3.1232-1238.2001

Morel, F., Frot-Coutaz, J., Aubel, D., Portalier, R., & Atlan, D. (1999). Characterization of a prolidase from lactobacillus delbrueckii subsp. bulgaricus CNRZ 397 with an unusual regulation of biosynthesis. *Microbiology (Reading, England), 145*(Pt 2), 437–446. https://doi.org/10.1099/13500872-145-2-437

Morelli, A., Massironi, A., Puppi, D., Creti, D., Domingo Martinez, E., Bonistalli, C., Fabroni, C., Morgenni, F., & Chiellini, F. (2019). Development of ulvan-based emulsions containing flavour and fragrances for food and cosmetic applications. *Flavour and Fragrance Journal, 34*(6), 411–425. https://doi.org/10.1002/ffj.3519

Murga-Garrido, S. M., Hong, Q., Cross, T.-W. L., Hutchison, E. R., Han, J., Thomas, S. P., … Rey, F. E. (2021). Gut microbiome variation modulates the effects of dietary fiber on host metabolism. *Microbiome, 9*(1), Article 117. https://doi.org/10.1186/s40168-021-01061-6

Oba, S., Washida, K., Shimada, Y., Sunagawa, T., Tanihiro, R., Sugiyama, H., & Nakamura, Y. (2020). Yeast mannan increases *bacteroides thetaiotaomicron* abundance and suppresses putrefactive compound production in in vitro fecal microbiota fermentation. *Bioscience, Biotechnology, and Biochemistry, 84*(10), 2174–2178. https://doi.org/10.1080/09168451.2020.1784704

Pang, Z., Lu, Y., Zhou, G., Hui, F., Xu, L., Viau, C., … Xia, J. (2024). MetaboAnalyst 6.0: Towards a unified platform for metabolomics data processing, analysis and interpretation. *Nucleic Acids Research, 52*(W1), W398–W406. https://doi.org/10.1093/nar/gkae253

Pérez-Burillo, S., Molino, S., Navajas-Porras, B., Valverde-Moya, Á. J., Hinojosa-Nogueira, D., López-Maldonado, A., … Rufián-Henares, J.Á. (2021). An in vitro batch fermentation protocol for studying the contribution of food to gut microbiota composition and functionality. *Nature Protocols, 16*(7), 3186–3209. https://doi.org/10.1038/s41596-021-00537-x

Procházková, N., Laursen, M. F., La Barbera, G., Tsekitsidi, E., Jørgensen, M. S., Rasmussen, M. A., … Roager, H. M. (2024). Gut physiology and environment explain variations in human gut microbiome composition and metabolism. *Nature Microbiology, 9*(12), 3210–3225. https://doi.org/10.1038/s41564-024-01856-x

Qi, Q., Li, J., Yu, B., Moon, J.-Y., Chai, J. C., Merino, J., … Kaplan, R. C. (2022). Host and gut microbial tryptophan metabolism and type 2 diabetes: An integrative analysis of host genetics, diet, gut microbiome and circulating metabolites in cohort studies. *Gut, 71*(6), 1095–1105. https://doi.org/10.1136/gutjnl-2021-324053

Roager, H. M., & Licht, T. R. (2018). Microbial tryptophan catabolites in health and disease. *Nature Communications, 9*(1), Article 3294. https://doi.org/10.1038/s41467-018-05470-4

Ruan, Q., Chen, Y., Wen, J., Qiu, Y., Huang, Y., Zhang, Y., … Zhao, C. (2023). Regulatory mechanisms of the edible alga ulva lactuca polysaccharide via modulation of gut microbiota in diabetic mice. *Food Chemistry, 409*, Article 135287. https://doi.org/10.1016/j.foodchem.2022.135287

Schmid, R., Heuckeroth, S., Korf, A., Smirnov, A., Myers, O., Dyrlund, T. S., … Pluskal, T. (2023). Integrative analysis of multimodal mass spectrometry data in MZmine 3. *Nature Biotechnology, 41*(4), 447–449. https://doi.org/10.1038/s41587-023-01690-2

Schymanski, E. L., Jeon, J., Gulde, R., Fenner, K., Ruff, M., Singer, H. P., & Hollender, J. (2014). Identifying small molecules via high resolution mass spectrometry: Communicating confidence. *Environmental Science & Technology, 48*(4), 2097–2098. https://doi.org/10.1021/es5002105

Seong, H., Bae, J.-H., Seo, J. S., Kim, S.-A., Kim, T.-J., & Han, N. S. (2019). Comparative analysis of prebiotic effects of seaweed polysaccharides laminaran, porphyran, and ulvan using in vitro human fecal fermentation. *Journal of Functional Foods, 57*, 408–416. https://doi.org/10.1016/j.jff.2019.04.014

Shalaby, M., & Amin, H. (2019). Potential using of ulvan polysaccharide from *Ulva lactuca* as a prebiotic in synbiotic yogurt production. *Journal of Probiotics & Health, 07*(01). https://doi.org/10.35248/2329-8901.19.7.208

Shimizu, G. D., Marubayashi, R. Y. P., & Goncalves, S. A. (2024). AgroR: Experimental statistics and graphics for agricultural sciences (version r package version 1.3.6) [computer software]. https://CRAN.R-project.org/package=AgroR.

Sinha, A. K., Laursen, M. F., Brinck, J. E., Rybtke, M. L., Hjørne, A. P., Procházková, N., … Licht, T. R. (2024). Dietary fibre directs microbial tryptophan metabolism via metabolic interactions in the gut microbiota. *Nature Microbiology, 9*(8), 1964–1978. https://doi.org/10.1038/s41564-024-01737-3

Sonnenburg, E. D., Zheng, H., Joglekar, P., Higginbottom, S. K., Firbank, S. J., Bolam, D. N., & Sonnenburg, J. L. (2010). Specificity of polysaccharide use in intestinal bacteroides species determines diet-induced microbiota alterations. *Cell, 141*(7), 1241–1252. https://doi.org/10.1016/j.cell.2010.05.005

Stülke, J., & Hillen, W. (1999). Carbon catabolite repression in bacteria. *Current Opinion in Microbiology, 2*(2), 195–201. https://doi.org/10.1016/S1369-5274(99)80034-4

Tamime, A. Y., & Robinson, R. K. (2007). 7—Biochemistry of fermentation. In A. Y. Tamime, & R. K. Robinson (Eds.), *Tamime and Robinson's yoghurt* (3rd ed., pp. 535–607). Woodhead Publishing. https://doi.org/10.1533/9781845692612.535.

Torres, P. B., Nagai, A., Jara, C. E. P., Santos, J. P., Chow, F., & Santos, D. Y. A. C. D. (2021). Determination of sulfate in algal polysaccharide samples: A step-by-step protocol using microplate reader. *Ocean and Coastal Research, 69*, Article e21021. https://doi.org/10.1590/2675-2824069.21-010pbt

Wang, G., Fan, Y., Zhang, G., Cai, S., Ma, Y., Yang, L., Wang, Y., Yu, H., Qiao, S., & Zeng, X. (2024). Microbiota-derived indoles alleviate intestinal inflammation and modulate microbiome by microbial cross-feeding. *Microbiome, 12*(1), 59. https://doi.org/10.1186/s40168-024-01750-y

Wilson, B., & Whelan, K. (2017). Prebiotic inulin-type fructans and galacto-oligosaccharides: Definition, specificity, function, and application in gastrointestinal disorders. *Journal of Gastroenterology and Hepatology, 32*(S1), 64–68. https://doi.org/10.1111/jgh.13700

Wobbrock, J. O., Findlater, L., Gergle, D., & Higgins, J. J. (2011). *The aligned rank transform for nonparametric factorial analyses using only anova procedures. Proceedings of the SIGCHI conference on human factors in computing systems, CHI '11, 143–146. Doi; 10.1145/1978942.1978963*.

Zonfrillo, B., Bellumori, M., Digiglio, I., Innocenti, M., Orlandini, S., Furlanetto, S., Khatib, M., Papini, A., Mainente, F., Zoccatelli, G., & Mulinacci, N. (2025). Multivariate optimization of ulvan extraction applying response surface methodology (RSM): The case of *Ulva lactuca* L. from Orbetello Lagoon. *Carbohydrate Polymers, 354*, Article 123340. https://doi.org/10.1016/j.carbpol.2025.123340

Zonfrillo, B., Bellumori, M., Truzzi, E., Khatib, M., Faraoni, P., Bertelli, D., Ranaldi, F., & Mulinacci, N. (2025). Ulvan as a source of oligosaccharides for biological applications: Enzymatic hydrolysis in a biocompatible medium. *Food Chemistry, 492*, Article 145618. https://doi.org/10.1016/j.foodchem.2025.145618

Zuffa, S., Schmid, R., Bauermeister, A., P. Gomes, P. W., Caraballo-Rodriguez, A. M., El Abiead, Y., … Dorrestein, P. C. (2024). MicrobeMASST: A taxonomically informed mass spectrometry search tool for microbial metabolomics data. *Nature Microbiology, 9*(2), 336–345. https://doi.org/10.1038/s41564-023-01575-9